Magnetic reversal in Dy-doped $DyFe_2/YFe_2$ superlattice films

G. B. G. Stenning,[1,2] G. J. Bowden,[1] P. A. J. de Groot,[1] G. van der Laan,[3] A. I. Figueroa,[3] P. Bencok,[4] P. Steadman,[4] and T. Hesjedal[4,5]

[1]*School of Physics and Astronomy, University of Southampton, SO17 1BJ, United Kingdom*
[2]*ISIS Neutron and Muon Source, Rutherford Appleton Laboratory, Didcot, OX11 0QX, United Kingdom*
[3]*Magnetic Spectroscopy Group, Diamond Light Source, Chilton, Didcot OX11 0DE, United Kingdom*
[4]*Diamond Light Source, Chilton, Didcot OX11 0DE, United Kingdom*
[5]*Clarendon Laboratory, University of Oxford, Oxford OX1 3PU, United Kingdom*

(Received 20 November 2014; revised manuscript received 28 January 2015; published 4 March 2015)

Reversible magnetic exchange springs can be formed in the magnetically soft YFe_2 layers of epitaxial $DyFe_2/YFe_2$ multilayer films. Here we show that the insertion of just two monolayers of $DyFe_2$, placed directly in the middle of the YFe_2 layers, brings about substantial changes. Results are presented for a Dy-doped (110)-oriented $[DyFe_2(60\text{Å})/YFe_2(120\text{ Å})/DyFe_2(8\text{ Å})/YFe_2(120\text{ Å})]_{15}$ multilayer film, measured at 100 K in fields of up to ± 10 T. Using bulk magnetometry, micromagnetic modeling, and Dy-specific x-ray magnetic circular dichroism, it is shown that Dy doping substantially increases the number of spin states available to the system. Altogether 12 distinct spring states are identified which bring additional complexity to the magnetic reversal process. In particular, the exchange springs are no longer reversible, exhibiting magnetic exchange-spring collapse. Full and partial magnetic loops are presented for fields applied along the in-plane easy [001] axis and the in-plane hard $[\bar{1}10]$ axis. In particular, it is demonstrated that exchange-spring collapse is sharpest when the field is applied along a hard in-plane $[\bar{1}10]$ axis.

DOI: 10.1103/PhysRevB.91.094403 PACS number(s): 68.65.Ac, 75.60.Ch, 75.30.Gw, 78.70.Dm

I. INTRODUCTION

Magnetic switching underpins much of today's technology from the design of permanent magnets, hard disk drives, magnetic read heads, to spintronic devices [1,2]. Here, we focus on modifying switching behavior in *exchange-spring magnets* [3–6]. Originally, the latter were proposed as a means of increasing the maximum energy product $(BH)_{\max}$ of permanent magnets. Such magnets consist of alternate hard and soft magnetic layers: The hard layers providing the coercivity whereas the soft or spring layers (usually iron) boost the overall magnetic moment. But there are other possible applications. Exchange-spring systems have been suggested as a means to overcome the *superparamagnetic* limit, encountered in the design of hard disk drives. The idea here is to use magnetic exchange springs, set up in the soft Fe layers, as spin-wave-assisted *magnetic levers* to switch hard adjacent layers [7–10]. Finally, we note that Ni doping of the exchange-spring system $(Co/Pd)_n/CoFeB$ has recently been used to fine-tune the magnetization directions in the $(Co/Pd)_n$ multilayer for possible applications in magnetoresistive random access memory technology [11].

Multilayers consisting of hard rare-earth Laves phase (R-Fe_2) layers, interleaved with magnetically soft YFe_2 layers, have proved to be excellent model systems for the study of magnetic exchange springs. For example, $DyFe_2/YFe_2$ multilayer films have been used to demonstrate exchange-spring-driven giant magnetoresistance [12] and negative coercivity [13]. In addition, Er-selective x-ray magnetic circular dichroism (Er-XMCD) experiments proved decisive in unraveling a double magnetic switching mechanism in an $ErFe_2/YFe_2$ multilayer at 200 K [14]. In this system bulk magnetic measurements reveal only a weak signature of a magnetic-double switch at ∼200 K [15]. By contrast, the Er-XMCD signal is much larger allowing a clear-cut explanation. The double switch originates from the magnetic anisotropy of the Er^{3+} ion, which is characterized by low-energy saddle points between two near-cubic ⟨111⟩ easy axes. As the magnetic field is increased, the balance of the magnetic exchange and Zeeman and anisotropy energies slips to and fro between in-plane and out-of-plane ⟨111⟩ axes, giving rise to a double magnetic switch.

More recently, Dy- and Fe-XMCD measurements have been used to provide a complete picture of magnetic switching in a $[DyFe_2(60\text{ Å})/YFe_2(240\text{ Å})]_{15}$ multilayer. Previously, magnetic reversal in this system, at low temperatures, has been described in terms of a single switch, from a reversed antiferromagnetic (AF) state to an in-plane magnetic exchange spring [16,17]. However, in practice, the magnetic reversal also involves an intermediate *transverse out-of-plane magnetic exchange spring* [18]. Thus magnetic reversal is characterized by a two-step process. The situation is further complicated if small amounts of Dy are introduced into the center of the YFe_2 springs. The exchange springs are no longer reversible and give rise to further steps in the hysteresis loops. This situation has also been examined by Wang *et al.* [19] using bulk magnetic measurements complemented by magnetic modeling using an object-oriented micromagnetic framework (OOMMF) [20].

In this paper, we investigate the Dy-doped $[DyFe_2(60\text{ Å})/YFe_2(240\text{ Å})]_{15}$ multilayer sample more incisively using element-selective Dy-XMCD. In addition, results are presented for fields applied along both in-plane hard and in-plane easy axes. As we will see, Dy-XMCD is an essential tool in identifying the large number of spin states available to the Dy-doped multilayer system. Specifically, magnetic reversal scenarios are presented for magnetic fields applied along the in-plane [001] easy axis and hard in-plane $[\bar{1}10]$ axis. The resulting spring configurations are not all identical, requiring separate discussions. A total of 12 different spin states are identified, and it is argued that the number of steps involved in the magnetic reversal process increases from three

in the undoped $DyFe_2/YFe_2$ multilayers up to five in the Dy-doped $DyFe_2/YFe_2$ superlattices.

II. EXPERIMENTAL DETAILS

The multilayers were grown by molecular-beam epitaxy (MBE) as detailed in Refs. [21,22]. A 100-Å-thick Nb buffer layer, followed by a 20-Å-thick Fe seed layer, were deposited onto an epiready $(11\bar{2}0)$ sapphire substrate, which was degreased prior to loading into the MBE system. The Laves phase material was subsequently grown in the (110) orientation with the major axes parallel to those of Nb. The latter was achieved by co-deposition of the elemental fluxes at a substrate temperature of 600 °C. The nominal composition of the superlattice is as follows:

$$[DyFe_2(60\ \text{Å})/YFe_2(120\ \text{Å})/DyFe_2(8\ \text{Å})/YFe_2(120\ \text{Å})]_{15}$$

Finally, to prevent oxidation, the multilayer was capped with 100 Å of Nb.

Bulk magnetic measurements were performed using superconducting quantum interference device (SQUID) magnetometry with a temperature range of 1.8–300 K and a field range of up to ±7 T. The fields were applied along an in-plane easy [001] axis and an in-plane hard $[\bar{1}10]$ axis.

X-ray absorption spectroscopy (XAS) was performed at the Diamond Light Source using the soft x-ray beamline I10, which is equipped with a 14-T superconducting magnet. The incident x-ray beam is always parallel to the magnetic field and has nearly 100% circular polarization. The Dy-$M_{4,5}$ absorption edges (e.g., Ref. [23]) were measured in fluorescence yield using one of the two available fluorescence detectors, parallel and perpendicular to the incident x-ray beam. A typical Dy-XMCD signal is shown in Fig. 1. Unfortunately, the Fe-XMCD signal suffered heavily from saturation effects and therefore provided little in the way of useful information (see, e.g., the discussion in Ref. [24]). At each value of the applied magnetic field, the Dy-$M_{4,5}$ XAS was measured at the photon energy of the absorption edge (indicated by the arrow in Fig. 1) as well as before the edge for both helicities of circular polarizations. To record hysteresis loops the magnetic field was swept between

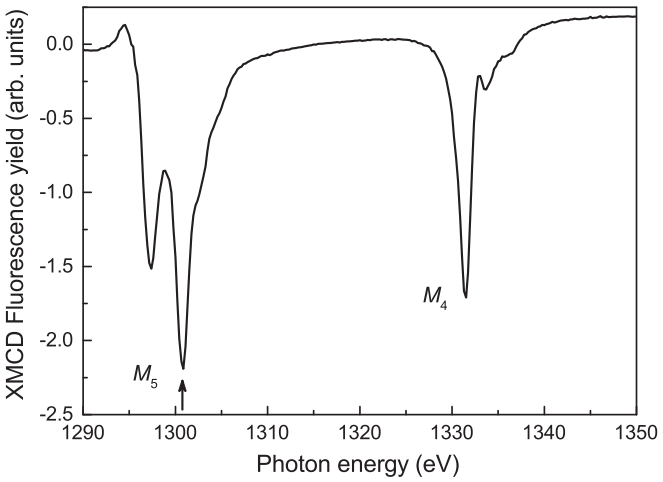

FIG. 1. Dy-$M_{4,5}$-XMCD measured using fluorescence yield detection. The vertical arrow indicates the photon energy used to record the Dy-XMCD hysteresis loops.

±10 T. For the in-plane [001] measurement, the sample was aligned with the [001] axis at 10° with respect to the magnetic field and x-ray beam to allow the latter to impinge on the surface of the sample. For the experiments described here, the temperature was set to 100 K to ensure that the easy axis of magnetization is the in-plane [001] axis [13,18].

III. EXPERIMENTAL RESULTS

A. Bulk magnetization

The bulk magnetization loops measured using a SQUID can be seen in Figs. 2 and 3. In Fig. 2, we see that the full loop (black curve) is very similar to the loop obtained for the undoped $DyFe_2/YFe_2$ multilayer [18]. For example, there is a clear two-step reversal process (at 3 and 4 T) in the first and third quadrants. In Ref. [18], it was argued that the first of these steps is characterized by a transverse out-of-plane exchange-spring state, whereas the second step is characterized by the Dy moments pointing along an in-plane easy [001] axis. [For those readers who do not have Ref. [18] on hand, look at Fig. 6(a)]. Additionally, negative coercivity is still present in the doped superlattice, but it is less pronounced. Here, we find a slight inflection in the slope of the magnetization as the loop passes through the zero field which is not present in the undoped sample. This is also evident in the partial loops shown in Fig. 2(b). Later when we examine the Dy-XMCD results, we will see that this small region of the M-B_a loop is characterized by a clear two-step process.

When the field is applied along a hard in-plane $[\bar{1}10]$ axis (Fig. 3), the loop is again characterized by: (i) a negative coercivity, (ii) an inflection point near $B_a = 0$ T, (iii) at least

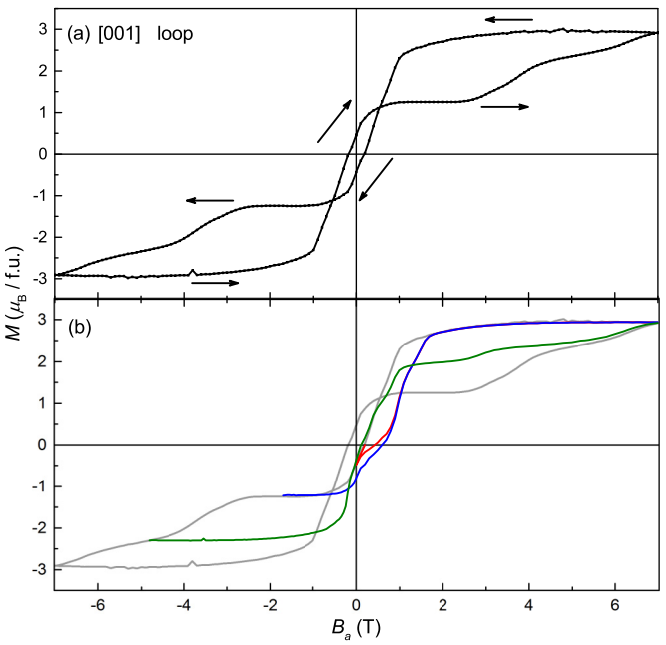

FIG. 2. (Color online) (a) SQUID magnetization loop at 100 K for a field directed along an in-plane [001] axis. The arrows indicate the direction of the field sweep. (b) Magnetization loop (gray curve) overlaid with partial loops: $+7 \rightarrow 0 \rightarrow 7$ T (red curve), $+7 \rightarrow -1.7 \rightarrow 7$ T (blue curve), and $+7 \rightarrow -4.8 \rightarrow 7$ T (green curve). Note that the red and blue curves largely overlap.

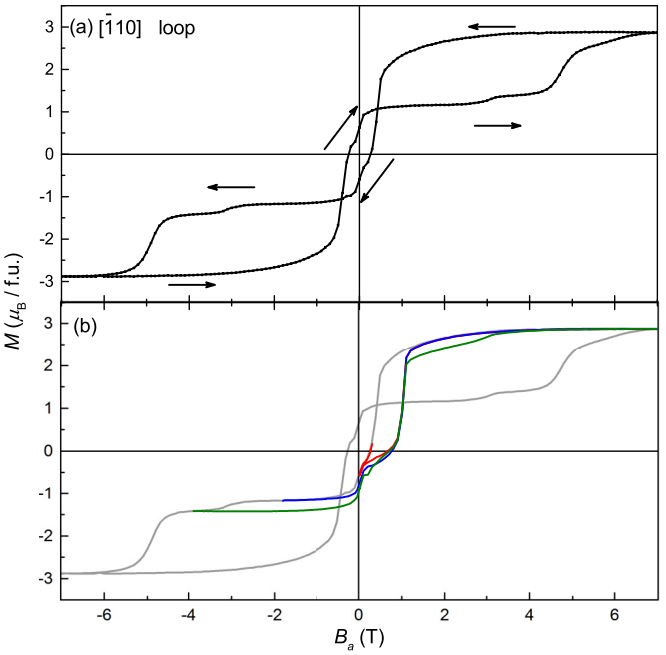

FIG. 3. (Color online) (a) SQUID magnetization loop at 100 K for a field directed along an in-plane [$\bar{1}10$] axis. The arrows indicate the direction of the field sweep. (b) Magnetization loop (gray curve) overlaid with partial loops: $+7 \rightarrow 0 \rightarrow 7$ T (red curve), $+7 \rightarrow -1.8 \rightarrow 7$ T (blue curve), and $+7 \rightarrow -3.9 \rightarrow 7$ T (green curve). Note that the red, blue, and green curves largely overlap.

three switching steps, and (iv) an exchange-spring collapse. As far as the latter is concerned, when the applied field is reduced from a large positive value to zero, the YFe_2 magnetic exchange springs unwind leading to a decrease in magnetization. However, from examination of Fig. 3 it is evident that the fall in the exchange-spring magnetization in the region of $\sim$1 T is precipitous. Here the anisotropic Dy ions in the center of the YFe_2 exchange springs hold up the unwinding of the exchange springs, until a critical field is reached, below which the exchange springs collapse into a

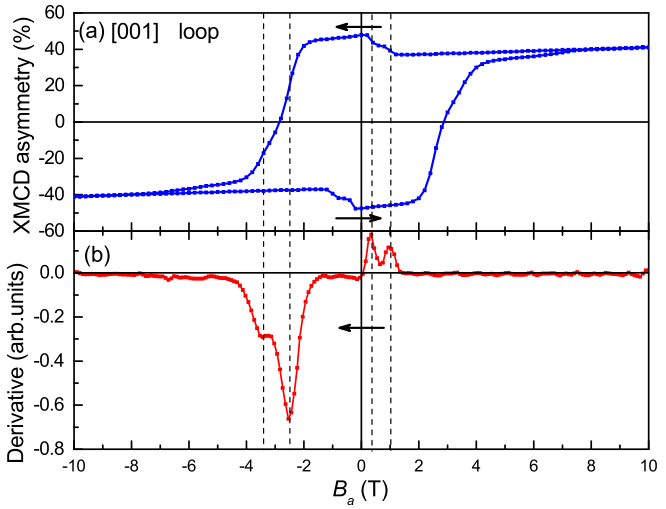

FIG. 4. (Color online) (a) Dy-XMCD loop for a field applied along an easy in-plane [001] axis. (b) The first derivative of the loop for decreasing magnetization.

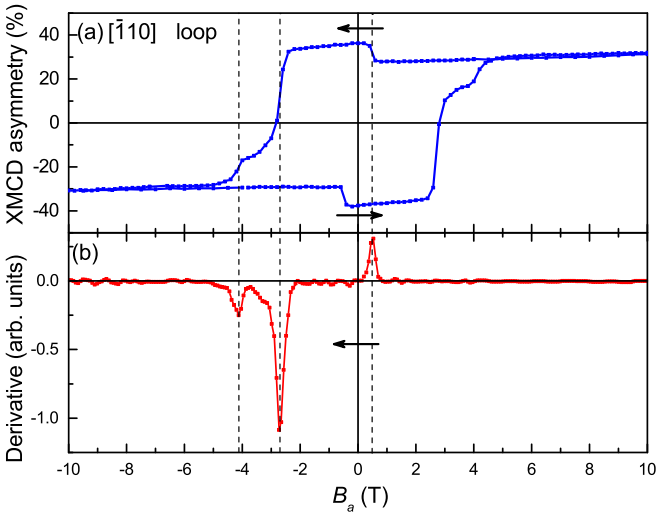

FIG. 5. (Color online) Dy-XMCD loop for a field applied along a hard in-plane [$\bar{1}10$] axis. (b) The first derivative of the loop for decreasing magnetization.

ferromagnetic state. Note that the exchange-spring collapse is much sharper when the field is applied along the hard [$\bar{1}10$] axis. It is also very evident, from an examination of the partial loops shown in Fig. 3(b), that the exchange-spring collapse region is very hysteretic. It can be described as a minor loop, positively shifted to $\sim+0.8$ T with a field width of $\sim$0.6 T.

In the past, researchers in the field have had to rely heavily on micromagnetic modeling to interpret such magnetization curves (see, e.g., Ref. [19]). Of course, this involves summing all the contributions from the Dy, Fe, and Y moments involved. However, nowadays, with the advent of element-selective XMCD, it is possible to look at some of the layers selectively. This confers significant advantages as we will see below.

B. Dy-XMCD results

The two principal Dy-XMCD loops for fields applied along the in-plane easy [001] axis and in-plane hard [$\bar{1}10$] axis can be seen in Figs. 4(a) and 5(a), respectively. In general, the loops are far from square. For example, there are two small steps in the region of $0 \rightarrow 1$ T in the first quadrant of Fig. 4(a). Clearly, several spin states are involved in the reversal process near $B_a = 0$ T. This conclusion is further strengthened by examining the first derivatives of the two loops in question. These are shown as red curves in Figs. 4(b) and 5(b), taken going from a positive to a negative field. The peaks in the derivative are evidence for a rapid change between one spin state to another.

We turn now to a discussion of the possible magnetization reversal mechanisms. In practice, it is necessary to treat each loop separately because of the differing spin states involved.

IV. MAGNETIC REVERSAL FOR FIELDS DIRECTED ALONG AN EASY IN-PLANE [001] AXIS

Magnetic reversal in an undoped $DyFe_2$(60 Å)/YFe_2(240 Å) multilayer has already been described [18]. For convenience, the basic steps in magnetic reversal for fields directed along the easy in-plane [001] axis are illustrated

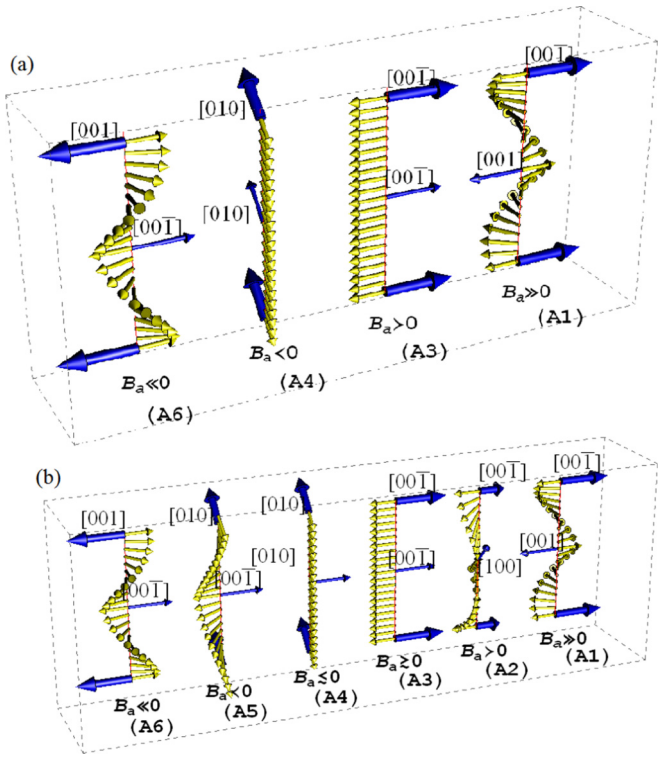

FIG. 6. (Color online) (a) A possible three-step magnetic reversal process in a Dy-doped $DyFe_2/YFe_2$ multilayer for fields directed along the easy in-plane [00$\bar{1}$] axis. Here the thick (thin) blue arrows represent the block (spring) 60-Å (8-Å) Dy layers, respectively. For ease of visualization, we have included two Dy block arrows in each diagram, however, strictly speaking only one is required per unit cell. (b) A plausible five-step magnetic reversal process for fields directed along an in-plane easy [00$\bar{1}$] axis (left to right). The proposed spin state sequence is only valid starting from a large positive field state (A1) and reducing to a large negative field state (A6).

schematically in Fig. 6(a). The thick single blue arrows represent the Dy moments in the 60-Å layers of Dy, whereas the thin blue arrows represent the 8 Å of Dy in the middle of the YFe_2 springs [hereafter referred to as Dy_B (block) and Dy_S (spring), respectively]. This reversal picture is essentially the same as that of Ref. [18], except for the presence of the additional Dy moments in the middle of the YFe_2 layer. In practice, we anticipate that the reversal procedure in the Dy-doped multilayer will be similar but with possible changes introduced by Dy doping in the YFe_2 springs.

First we note that the hysteretic steps outlined in Fig. 6(a) only apply for magnetic fields reducing from a large positive to a negative field, i.e., from $+10 \rightarrow -10$ T. In a large positive applied field the state can be described as Dy_B [00$\bar{1}$]/Dy_S [001], [see (A1) in Fig. 6(a)]. Here, the subscripts B (S) are shorthand notation for block (spring), respectively. This state is characterized by a large exchange spring in the YFe_2 layer which maximizes the overall magnetic moment in the direction of the applied field. Here the Dy moments in the block layers (60 Å) are aligned parallel to the direction of the applied field, whereas the Dy moments in the middle of the YFe_2 spring (8 Å) are obliged due to the strong Dy-Fe AF magnetic exchange to point in the opposite direction. As the field is reduced in magnitude, the magnetic springs in the YFe_2 layers unwind, and the spin system eventually collapses in a small positive field into a net AF state Dy_B [00$\bar{1}$]/Dy_S [00$\bar{1}$] [cf. (A3) in Fig. 6(a)]. At this point in the magnetization cycle, the net magnetic moment is negative [calculated value of $-0.93\mu_B$ per formula unit (f.u.) at 100 K], hence the use of the term negative coercivity [13]. As the field is swept to negative values, the net AF state becomes unstable and switches to an out-of-plane Dy_B[010]/Dy_S[010] *transverse spring state*, first identified in Ref. [18] [cf. (A4) in Fig. 6(a)]. Finally, in large negative fields the out-of-plane state switches to the in-plane Dy_B[001]/Dy_S[00$\bar{1}$] [cf. (A6) in Fig. 6(a)], the reverse of what is observed in a large positive field.

It is not difficult to see how additional steps can be incorporated into the basic scheme outlined in Fig. 6(a). For example, the step between the spiral state Dy_B[00$\bar{1}$]/Dy_S[001] (A1) to the net AF state Dy_B[00$\bar{1}$]/Dy_S[00$\bar{1}$] (A3) could be modified to include an intermediate state Dy_B[00$\bar{1}$]/Dy_S[100] (A2). Here the Dy moments in the spring jump into an out-of-plane [100] axis, leaving the Dy moments in the block still aligned along the in-plane [00$\bar{1}$] axis. Similarly, an additional state Dy_B[010]/Dy_S[00$\bar{1}$] (A5) could be inserted between the out-of-plane state Dy_B[010]/Dy_S[010] (A4) and the final in-plane state Dy_B[001]/Dy_S[00$\bar{1}$] (A6). In this intermediate state, the out-of-plane [010] Dy moments in the spring switch to the in-plane [00$\bar{1}$] axis leaving the Dy moments in the block still aligned along the out-of-plane [010] axis. A revised reversal process is summarized schematically in Fig. 6(b). For advice we turn next to micromagnetic modeling.

V. MICROMAGNETIC MODELING

The model used in this paper has been described previously [14], so here we give just a brief summary of the model. The cubic Laves R-Fe_2 compounds are characterized by a strong ferromagnetic Fe-Fe exchange B_{Ex}(Fe-Fe) $\approx$ 600 K, which runs throughout the entire lattice. This interaction is primarily responsible for the high Curie temperatures. Next in magnitude is the AF Dy-Fe exchange field B_{Ex}(Dy-Fe) $\approx$ 100 K at $T = 0$ K. Here we adopt a three-component magnetic model with the Dy, Y, and Fe magnetic moments set at $10\mu_B$, $0\mu_B$, and $1.5\mu_B$, respectively, at $T = 0$ K [25]. Of course, this model is a gross oversimplification. Band-structure calculations reveal that there are induced $R\,5d$ moments in addition to the Fe $3d$ moments [26]. However, since the $R\,5d$ moments are driven primarily by the Fe $3d$ sublattice, it is a reasonable approximation to use a discrete two-component R-Fe model, provided we ascribe say $\mu_{Dy} = 10\mu_B$ and $\mu_{Fe}(= \mu_{3d} + \mu_{5d}) = 1.5\mu_B$.

In general, the model yields not only the magnitudes and directions of all the magnetic moments involved, but also their energies. The latter can be useful in deciding which is the preferred spin state at a given temperature and magnetic field. However the reader is warned that in the Dy-doped $DyFe_2/YFe_2$ multilayer many different spin states are involved, all of which are dependent on the parameters used in the model. In the past, the latter has been used fairly successfully to interpret one- or two-step reversal processes. For example, it is well known that most models overestimate the value of the switching field (Brown's paradox [27]). For

example, using the micromagnetic simulation code OOMMF [20] estimates of the switching fields in the Dy-doped multilayer are at least an order of magnitude larger than the experimental values (see the discussion in Ref. [19]). To some extent, these overestimates can be corrected by calculating *both* the switching and the energy crossover fields and estimating the actual switching field by taking their average [14]. However, in the present situation, many more spring states are involved, and although every care has been taken to obtain the best estimates for the exchange and magnetic anisotropy parameters, small variations can make large differences as we will see below. Instead, therefore, we choose to use the micromagnetic model primarily as a guide for the interpretation of the experimental results.

VI. MODELING RESULTS FOR A FIELD DIRECTED ALONG AN IN-PLANE EASY [001] AXIS

Using the model described above, the five distinct states illustrated schematically in Fig. 6(b) (A1) → (A6) were indeed found to be stable. Their field ranges are listed in Table I. We denote the upper and lower field ranges as the Stoner-Wohlfarth limits. Some readers might find the use of such terminology strange. In the past, the Stoner-Wohlfarth limit (or switching field) was generally discussed in the context of a homogeneous magnet, involving at most one or two variables. However, here we are dealing with model domain walls, involving many more parameters. Nevertheless, in principle, the switching limits are determined in exactly the same way. In the conventional Stoner-Wohlfarth magnet, with say just one parameter θ, stability or otherwise is determined by the properties of the double differential $\partial^2 E/\partial\theta^2$, where E is the sum of the Zeeman and anisotropy energies. In the case of an exchange-spring system, the stability of a given spin configuration is again determined by the double differential of the energy but this time spanned by many more variables. Here stability is determined by the eigenvalues of the double differential energy matrix $\boldsymbol{E''}$ [17]. If just one of the eigenvalues of $\boldsymbol{E''}$ goes soft, the spin configuration is no longer stable. It must perforce collapse into a differing spin state.

From Table I, it is clear that there is a considerable overlap between the field ranges of the six spin states in question. As a result, construction of a calculated magnetic loop is difficult. In particular, it is not even clear from Table I, which is the ground state in a large positive field. However, given previous experience with the undoped $DyFe_2/YFe_2$ multilayer [18], we expect $Dy_B[00\bar{1}]/Dy_S[001]$ (A1) to be the preferred ground state. Nevertheless, the neighboring $Dy_B[00\bar{1}]/Dy_S[100]$ (A2) state is surprisingly robust, being stable over a large field range of $-55.10 \leqslant B_a < (50+)\ T$.

TABLE I. Calculated Stoner-Wohlfarth limits at 100 K for the spin states (A1) → (A6) of Fig. 6(b) with the field applied along an in-plane $[00\bar{1}]$ easy axis.

State		Field range (T)
$Dy_B[00\bar{1}]/Dy_S[001]$	(A1)	$-1.62 \leqslant B_a < (50+)$
$Dy_B[00\bar{1}]/Dy_S[100]$	(A2)	$-55.10 \leqslant B_a < (50+)$
$Dy_B[00\bar{1}]/Dy_S[00\bar{1}]$	(A3)	$-55.10 \leqslant B_a < 1.54$
$Dy_B[010]/Dy_S[010]$	(A4)	$-18.74 \leqslant B_a < 18.74$
$Dy_B[010]/Dy_S[00\bar{1}]$	(A5)	$-18.74 \leqslant B_a < 2.09$
$Dy_B[001]/Dy_S[00\bar{1}]$	(A6)	$-(50+) \leqslant B_a < 1.62$

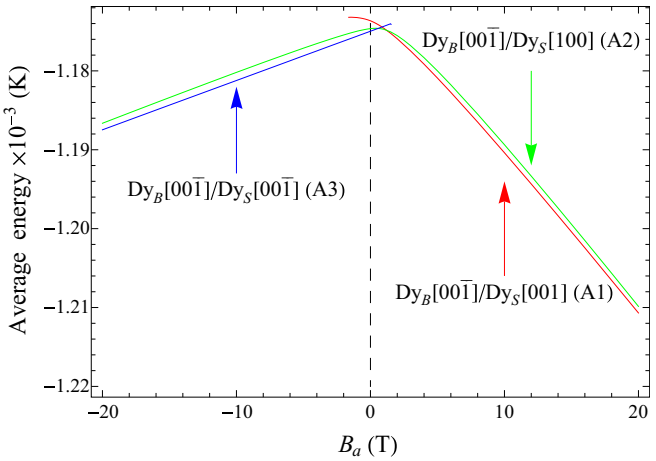

FIG. 7. (Color online) Average energy per formula unit versus magnetic field for the first three states of Fig. 6(b) (A1) → (A3). Only three states are shown for clarity.

To resolve this conundrum, we turn next to a discussion of the calculated average energy per formula unit of the spin states. In practice, the state with the lowest energy is likely to be the preferred state. The energies of the first three states in Fig. 6(b) [(A1) → (A3)] can be seen in Fig. 7 as a function of the magnetic field. From an examination of this diagram it is immediately clear that in a large positive field the energies of the $Dy_B[00\bar{1}]/Dy_S[001]$ (A1) and $Dy_B[00\bar{1}]/Dy_S[100]$ (A2) states are practically identical. Indeed, small changes in the parameters of the micromagnetic model used here could easily reverse the order of these two states. Thus the nature of the ground state in a large field remains uncertain.

Next, we examine the net magnetic moment of the states in question. In general, the state with the largest overall moment in a large positive field is likely to be the preferred ground state. The results can be seen in Fig. 8. Very surprisingly, in high magnetic fields the magnetic moments of the two states in question are almost identical with the intermediate state $Dy_B[00\bar{1}]/Dy_S[100]$ (A2) winning out slightly. Once again therefore, the nature of the ground state is uncertain.

Next we turn to the net Dy moment per spin state. The results for the five states in question can be seen in Fig. 9.

From Fig. 9 it is immediately clear that we should be able to distinguish between the first three states of Fig. 6(b) [(A1) →(A3)]. The largest (smallest) Dy moment $\sim 9\mu_B(\sim 7\mu_B)$ is associated with the net AF state $Dy_B[00\bar{1}]/Dy_S[00\bar{1}]$ (A3) $\{Dy_B[00\bar{1}]/Dy_S[001]$ (A1)$\}$, respectively, with the intermediate state $Dy_B[00\bar{1}]/Dy_S[100]$ (A2) somewhere in between. Indeed, this information can be used to interpret the experimental Dy-XMCD loop of Fig. 4. We draw the following conclusions. On starting from a large positive field the ground state is indeed $Dy_B[00\bar{1}]/Dy_S[001]$ (A1) as expected from the undoped case [18]. As the field is reduced, the intermediate spin configuration $Dy_B[00\bar{1}]/Dy_S[010]$ (A2) is accessed at ∼1.0 T. Finally, in a very small positive field the spring collapses to form the

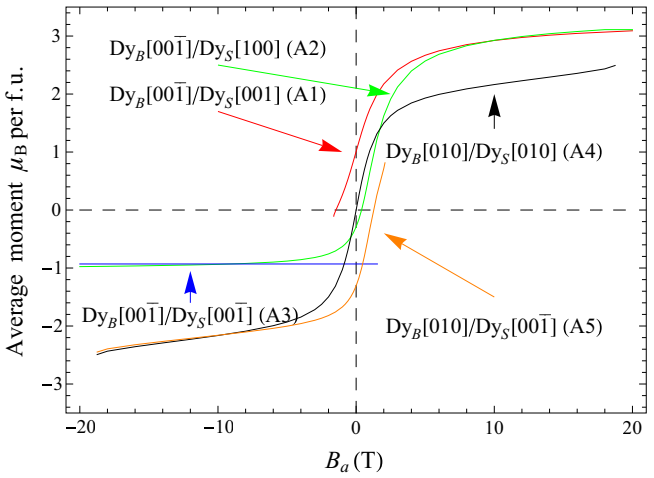

FIG. 8. (Color online) Net magnetic moment (μ_B per formula unit) versus applied field for the spring states shown in Fig. 6(b). Note that the response of the transverse spring state $Dy_B[010]/Dy_S[010]$ (A4) (black curve) is symmetric.

simple AF state $Dy_B[00\bar{1}]/Dy_S[00\bar{1}]$ (A3). Small hysteretic partial loops, shown as the blue and red curves in Fig. 10, confirm this interpretation. Both loops are hysteretic.

These conclusions are in agreement with the OOMMF calculations of Ref. [19] However, it should be noted that the latter used anisotropy parameters appropriate for 150 K instead of 100 K. This choice is questionable given that the direction of easy magnetization starts to move away from the easy [001] axis at temperatures above 100 K [13]. The latter also found hysteresis in partial loops obtained using bulk magnetometry but had to rely on OOMMF simulations for interpretation. By contrast, element-selective Dy-XMCD allows clear experimental signatures of the various spin states involved as the field is reduced from a large positive field to zero,

$$Dy_B[00\bar{1}]/Dy_S[001]\ (A1) \rightarrow Dy_B[00\bar{1}]/Dy_S[100]\ (A2) \rightarrow Dy_B[00\bar{1}]/Dy_S[00\bar{1}]\ (A3)$$

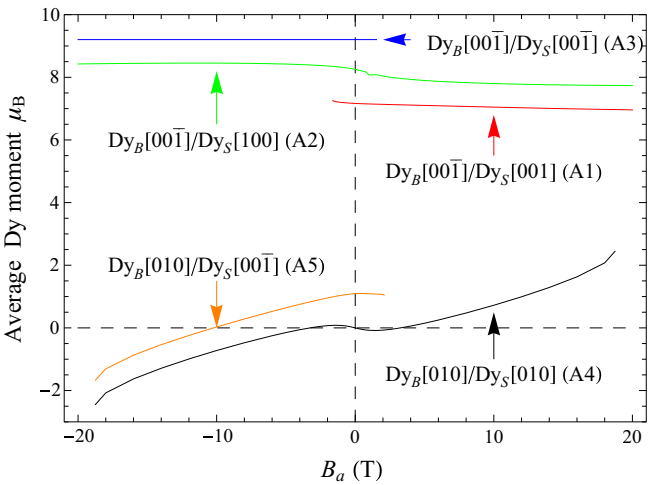

FIG. 9. (Color online) Average Dy magnetic moment versus applied field for the states shown in Fig. 6(b).

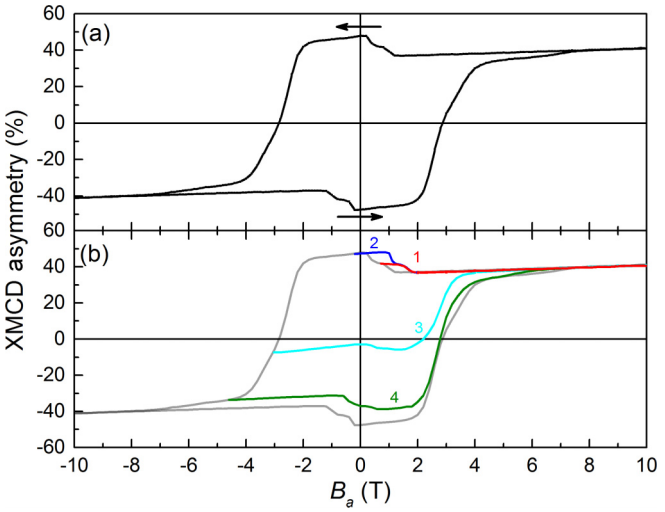

FIG. 10. (Color online) Dy-XMCD loop and partial loops for a field applied along an easy in-plane [001] axis. The partial loops were obtained using $10 \rightarrow 0.717 \rightarrow 10$ T (red curve), $10 \rightarrow -0.2 \rightarrow 10$ T (blue curve), $10 \rightarrow -3.025 \rightarrow 10$ T (cyan curve), and $10 \rightarrow -4.8 \rightarrow 10$ T (green curve), respectively, before returning to a large positive field.

The other partial loops shown in Fig. 10 can also be used to shed light on the other states accessed during magnetic reversal. For example, the curve obtained by sweeping the magnetic field from a large positive value to -3.025 T (cyan curve), and then back again, shows that the net Dy moment is close to zero when $B_a = 0$. This is clear evidence for the transverse exchange-spring state $Dy_B[010]/Dy_S[010]$ (A4). Here all the spins are perpendicular to the x-ray beam, so the Dy-XMCD signal should vanish.

Finally, the partial loop obtained by sweeping from a large positive field to $B_a = -4.8$ T can be used to illustrate an important point, so far left out of the discussion. In practice, the field is applied 10° away from the [001] axis to allow the x-ray beam to strike the surface of the film (see the Experimental section). So for positive fields, the favored transverse exchange-spring state is characterized by $Dy_B[100]/Dy_S[100]$. But if the field is swept from a large negative field back towards zero, the preferred transverse spring state should be $Dy_B[010]/Dy_S[010]$ (A4), again as shown in Fig. 6(b). So if the Dy moments in the spring fail to tunnel from the [100] to the [010] axis when the magnetic field goes negative, they will be forced to rotate from the [100] to the [010] axis in higher magnetic fields. We believe that this could be happening in the region of $-4.8 \rightarrow -7$ T where there is evidence of a slow rotation of the Dy signal towards saturation. Clearly, this portion of the magnetic loop will repay further investigation using either selective rotations of the film and/or history-dependent field cycling.

VII. MODELING RESULTS FOR FIELDS DIRECTED ALONG AN IN-PLANE HARD [$\bar{1}$10] AXIS

An early interpretation of the magnetic reversal process in an undoped $DyFe_2/YFe_2$ multilayer has been given in Ref. [28] but only in terms of one step between two spin states. In the case of the doped multilayer many more spin

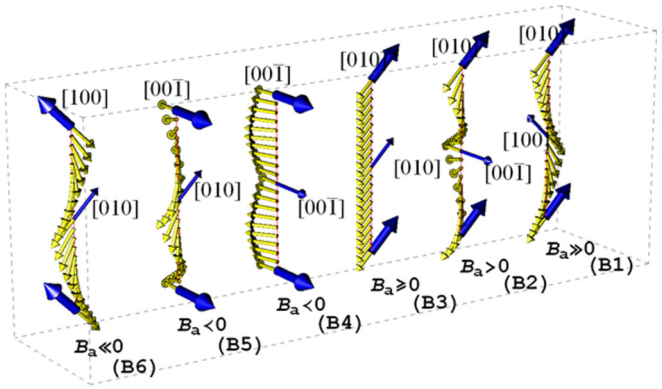

FIG. 11. (Color online) A plausible five-step mechanism for magnetic reversal for fields applied along an in-plane hard [$\bar{1}$10] axis (left to right). Note that the proposed sequence of steps only holds when starting from a large positive field (B1) and subsequently reducing the field to a large negative value (B6).

states can be expected. A plausible five-step reversal process for fields applied along an in-plane hard [$\bar{1}$10] axis can be seen in Fig. 11.

The five distinct states illustrated schematically in Fig. 11 were found to be stable. Their calculated Stoner-Wohlfarth limits are listed in Table II.

Once again, based on the information shown in Table II, it is difficult to decide on the preferred ground state in large applied magnetic fields. Both the $Dy_B[010]/Dy_S[100]$ (B1) and the $Dy_B[010]/Dy_S[00\bar{1}]$ (B2) spin configurations possess very similar energies and magnetic moments as illustrated in Figs. 12 and 13, respectively.

However, once again, the net Dy moment can be used to distinguish between the three field states [(B1) → (B3)] of Fig. 11 (see Fig. 14).

Starting from the right (B1), all the spins are confined to a plane perpendicular to the [00$\bar{1}$] axis (no x component). As such, the spins are all out of plane. Note that: (i) the springs can be described in terms of two 90° springs, and (ii) the net Dy component in the y direction is given by

$$\overline{\mu^{y}_{\mathrm{Dy}}} \sim \mu_{\mathrm{Dy}} \frac{15}{19\sqrt{2}} = 0.558\mu_{\mathrm{Dy}}\{\mathrm{Dy_B[010]/Dy_S[100]\ (B1)}\}. \tag{1}$$

As the field is reduced, the spring unwinds until a critical field is reached where the Dy moments in the YFe_2 springs

TABLE II. Calculated Stoner-Wohlfarth limits at 100 K for the spin states (B1) → (B6) of Fig. 11 for fields applied along an in-plane hard [$\bar{1}$10] axis.

State		Field range (T)
$Dy_B[010]/Dy_S[100]$	(B1)	$-4.33 \leqslant B_a < (50+)$
$Dy_B[010]/Dy_S[00\bar{1}]$	(B2)	$-21.93 \leqslant B_a < (50+)$
$Dy_B[010]/Dy_S[010]$	(B3)	$-21.93 \leqslant B_a < 4.64$
$Dy_B[00\bar{1}]/Dy_S[00\bar{1}]$	(B4)	$-17.53 \leqslant B_a \leqslant 17.53$
$Dy_B[00\bar{1}]/Dy_S[010]$	(B5)	$-17.53 \leqslant B_a \leqslant 4.24$
$Dy_B[100]/Dy_S[010]$	(B6)	$-(50+) \leqslant B_a \leqslant 4.33$

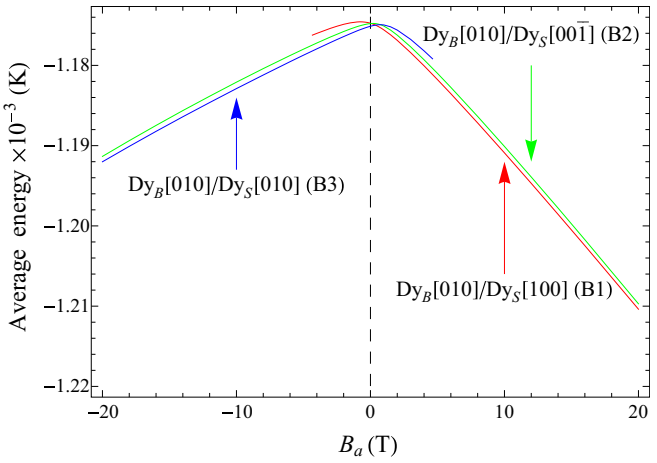

FIG. 12. (Color online) Average energy per formula unit versus magnetic field for the (B1) → (B3) states of Fig. 11. Only three states are shown for clarity.

suddenly switch to a new [00$\bar{1}$] axis, i.e., state (B2). Here the net Dy moment is given by

$$\overline{\mu^{y}_{\mathrm{Dy}}} \sim \frac{17}{19\sqrt{2}}\mu_{\mathrm{Dy}} = 0.633\mu_{\mathrm{Dy}}\{\mathrm{Dy_B[010]/Dy_S[00\bar{1}]\ (B2)}\}. \tag{2}$$

In a small positive field, the spring suddenly collapses, and the spin configuration adopts a simple AF state, i.e., state (B3). Here the Dy-XMCD signal should reach a maximum given that

$$\overline{\mu^{y}_{\mathrm{Dy}}} \sim \frac{1}{\sqrt{2}}\mu_{\mathrm{Dy}} = 0.707\mu_{\mathrm{Dy}}\{\mathrm{Dy_B[010]/Dy_S[010]\ (B3)}\}. \tag{3}$$

We can draw the following conclusion by comparing the predictions of Eqs. (1)–(3) with the experimental results of Fig. 5 . It would appear that unlike the results for fields applied along the [001] axis, there is no evidence for a two-step process as the applied field along the hard [$\bar{1}$10] axis is reduced from a large positive value to zero. In contrast, the Dy-XMCD

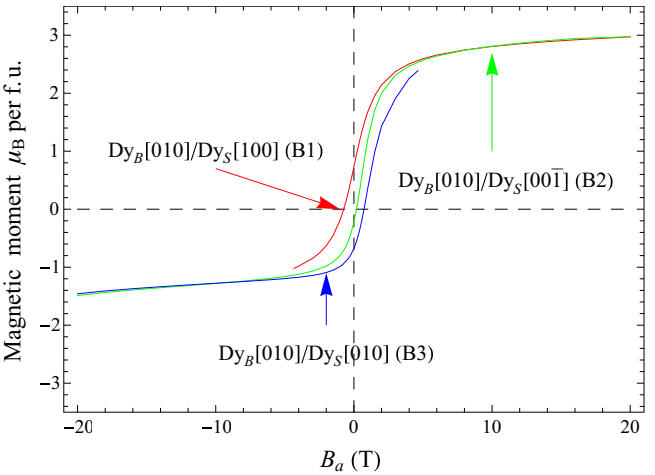

FIG. 13. (Color online) Net magnetic moment (μ_B per formula unit) versus magnetic field for the (B1) → (B3) states of Fig. 11. Only three states are shown for clarity.

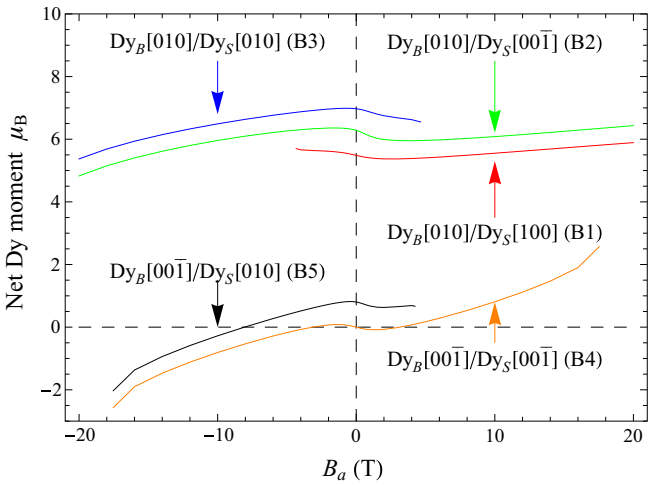

FIG. 14. (Color online) Average Dy magnetic moment for the states shown in Fig. 11 (B1) → (B5). Note the symmetric response of the transverse spring state Dy$_B$[00$\bar{1}$]/Dy$_S$[00$\bar{1}$] (B4) configuration.

evidence suggests a single step,

$$\text{Dy}_B[010]/\text{Dy}_S[100]\ (\text{B1}) \rightarrow \text{Dy}_B[010]/\text{Dy}_S[010]\ (\text{B3}),$$

thereby giving rise to a much sharper exchange-spring collapse.

Finally, there is clear evidence in the Dy-XMCD loop for a stable state at −4 T. We tentatively ascribe the transverse exchange-spring state Dy$_B$[00$\bar{1}$]/Dy$_S$[00$\bar{1}$] (B4) to this point in the hysteresis loop, which may subsequently collapse directly into the (B6) state without accessing (B5). As with the [001] results, this part of the magnetic loop needs more experimentation, taking into account the fact that the 10° misalignment of the sample may play a role.

VIII. CONCLUSIONS AND DISCUSSION

The properties of a Dy-doped $DyFe_2/YFe_2$ multilayer layer system have been investigated using bulk magnetometry and Dy-XMCD, complemented by micromagnetic modeling. Detailed scenarios of magnetic reversal for fields applied along both an easy and a hard in-plane axis have been presented and discussed. In particular, the inclusion of small amounts of Dy in the middle of the soft YFe_2 magnetic springs brings about additional complexity. This includes the phenomenon of *exchange-spring collapse*, which is more precipitous for fields applied along a hard [$\bar{1}$10] axis. In all, 12 different spin states have been identified/classified, offering increased opportunities in spin-wave-assisted magnetic reversal. In addition, it has been noted that there is considerable competition between differing spin states in the determination of the actual ground state, even in large applied magnetic fields. For example, for fields applied along an easy [00$\bar{1}$] axis, the energies and magnetic moments of the expected Dy$_B$[00$\bar{1}$]/Dy$_S$[001] (A1) and the unexpected Dy$_B$[00$\bar{1}$]/Dy$_S$[100] (A2) spin configurations are almost identical. Clearly, opportunities exist for the preparation of *metastable exchange-spring states*, either by applying the field at an angle away from the easy [00$\bar{1}$] axis, and/or by history-dependent procedures [29].

ACKNOWLEDGMENT

We acknowledge the Diamond Light Source for beamtime on I10 under Proposal No. SI-9875.

[1] C. Chappert, A. Fert, and F. Nguyen Van Dau, Nature Mater. **6**, 813 (2007).
[2] S. S. P. Parkin, M. Hayashi, and L. Thomas, Science **320**, 190 (2008).
[3] E. F. Kneller and R. Hawig, IEEE Trans. Magn. **27**, 3588 (1991).
[4] R. Skomski and J. M. D. Coey, IEEE Trans. Magn. **29**, 2860 (1993).
[5] R. Skomski and J. M. D. Coey, Phys. Rev. B **48**, 15812 (1993).
[6] R. Skomski, J. Appl. Phys. **76**, 7059 (1994).
[7] J. Zhang, Y. K. Takahashi, R. Gopalan, and K. Hono, Appl. Phys. Lett. **86**, 122509 (2005).
[8] D. Suess, T. Schrefl, S. Fahler, M. Kirchner, G. Hrkac, F. Dorfbauer, and J. Fidler, Appl. Phys. Lett. **87**, 012504 (2005).
[9] D. Suess, T. Schrefl, M. Kirchner, G. Hrkac, F. Dorfbauer O. Ertl, and J. Fidler, IEEE Trans. Magn. **41**, 3166 (2005).
[10] D. Suess, J. Magn. Magn. Mater. **308**, 183 (2007).
[11] T. N. Anh Nguyen, R. Knut, V. Fallahi, S. Chung, Q. Tuan Le, S. M. Mohseni, O. Karis, S. Peredkov, R. K. Dumas, Casey W. Miller, and J. Åkerman, Phys. Rev. Appl. **2**, 044014 (2014).
[12] S. N. Gordeev, J.-M. L. Beaujour, G. J. Bowden, B. D. Rainford, P. A. J. de Groot, R. C. C. Ward, M. R. Wells, and A. G. M. Jansen, Phys. Rev. Lett. **87**, 186808 (2001).
[13] J.-M. L. Beajour, S. N. Gordeev, G. J. Bowden, P. A. J. de Groot, B. D. Rainford, R. C. C. Ward, and M. R. Wells, Appl. Phys. Lett. **78**, 964 (2001).
[14] G. B. G. Stenning, A. R. Buckingham, G. J. Bowden, R. C. C. Ward, G. van der Laan, L. R. Shelford, F. Maccherozzi, S. S. Dhesi, and P. A. J. de Groot, Phys. Rev. B **84**, 104428 (2011).
[15] K. N. Martin, C. Morrison, G. J. Bowden, P. A. J. de Groot, and R. C. C. Ward, Phys. Rev. B **78**, 172401 (2008).
[16] J. P. Zimmermann, G. Bordignon, R. P. Boardman, T. Fishbacher, and H. Fangohr, J. Appl. Phys. **99**, 08B904 (2006).
[17] G. J. Bowden, J.-M. L. Beaujour, A. A. Zhukov, B. D. Rainford, P. A. J. de Groot, R. C. C. Ward, and M. R. Wells, J. Appl. Phys. **93**, 6480 (2003).
[18] G. B. G. Stenning, G. J. Bowden, S. A. Gregory, J.-M. L. Beaujour, P. A. J de Groot, G. van der Laan, L. R. Shelford, P. Bencok, P. Steadman, A. N. Dobrynin, and T. Hesjedal, Appl. Phys. Lett. **101**, 072412 (2012).
[19] D. Wang, A. R. Buckingham, G. J. Bowden, R. C. C. Ward, and P. A. J. de Groot, Mater. Res. Express **1**, 036110 (2014).
[20] OOMMF:http:/math.nist.gov/oommf.
[21] M. J. Bentall, R. C. C. Ward, E. J. Grier, and M. R. Wells, J. Phys.: Condens. Matter **15**, 6493 (2003).

[22] C. Wang, A. Kohn, S. G. Wang, and R. C. C. Ward, J. Phys.: Condens. Matter **23**, 116001 (2011).
[23] B. T. Thole, G. van der Laan, and G. A. Sawatzky, Phys. Rev. Lett. **55**, 2086 (1985).
[24] G. van der Laan and A. I. Figueroa, Coord. Chem. Rev. **277-278**, 95 (2014).
[25] G. J. Bowden, A. R. Buckingham, G. B. G. Stenning, and P. A. J. de Groot, J. Phys.: Condens. Matter **22**, 291001 (2010).
[26] M. S. S. Brooks, L. Nordstrom, and B. Johansson, J. Phys.: Condens. Matter **3**, 2357 (1991).
[27] W. F. Brown, Rev. Mod. Phys. **17**, 15 (1945).
[28] D. Wang, A. R. Buckingham, G. J. Bowden, R. C. C. Ward, and P. A. J. de Groot, *36th Annual Condensed Matter and Materials Meeting, Wagga Wagga, New South Wales, 2012* (Charles Sturt University, Wagga Wagga, New South Wales, Australia, 2012), p. TP16.
[29] G. B. G. Stenning, G. J. Bowden, S. A. Gregory, P. A. J. de Groot, G. van der Laan, L. R. Shelford, P. Bencok, P. Steadman, A. N. Dobrynin, and T. Hesjedal, Phys. Rev. B **86**, 174420 (2012).